

Plume Characterization of an Ion Focusing Hall Thruster

Kunning G. Xu¹ and Mitchell L.R. Walker²

High-Power Electric Propulsion Laboratory, Georgia Institute of Technology, Atlanta, GA 30332 USA

The T-220HT is a 10-kW class Hall effect thruster developed as the primary propulsion system for satellites. In-channel electrodes and additional magnetic coils are added to study ion focusing to decrease energy losses from ion-wall neutralization and plume divergence in order to increase the thrust-to-power ratio. In this study, electrically-biased graphite electrode rings are embedded in the discharge channel walls to repel radial ions. The thruster is tested from 125-300 V at 9 A discharge, with the electrodes either floating, biased to 10 V or 30 V. The mass flow rate was varied from 9.8-10.4 mg/s to maintain constant current. Maximum chamber pressure was 1.5e-5 Torr-Xe. Performance measurements on xenon show a maximum increase in thrust-to-power ratio of 4.84 mN/kW, 15.3 mN thrust, 206 s I_{sp} , and 8% anode efficiency. The plume ion current density, ion energy distribution function, and plasma potential is characterized and indicates a collimation of the ion beam and a increase in ion number density without an increase in propellant neutrals, which results in an increase in mass utilization. The different electrode currents and ion energy distribution functions at 10 V compared to 30 V electrodes leads to the idea of different modes of operation with different electrode biases.

I. Introduction

HALL effect thrusters (HET) are one of the prime candidates for use as primary propulsion systems for satellites. They provide a combination of thrust and specific impulse (I_{sp}) that offers advantages for many near Earth missions. They have been studied in both Russia and the US and their performance has been demonstrated in laboratory tests. Current space propulsion demands a higher thrust-to-power (T/P) ratio for shorter burn times and quicker orbit changes. Operating a HET at high T/P ratios requires a low discharge voltage and high discharge current for efficiency operations. As the discharge current increases, the ion density increases and the number lost to the discharge channel wall also increases, which decreases efficiency. Thus, to increase the efficiency at high T/P requires a reduction in ion-wall collisions. The goal of this research is to reduce such collisions through the use of ion focusing technology in the discharge chamber. The ion focusing guides ions with trajectories intersecting the chamber wall towards the centerline of the chamber, which results in an increase in efficiency and T/P .

Current developments in high T/P Hall thrusters have yielded many designs. Thrusters such as the NASA-173M from Michigan, Busek's BHT-1000, Aerojet's BPT-4000, and the 6 kW Hall thruster at Michigan generate high T/P levels at low voltages.^{1, 3-5} The BHT-1000 show the highest of 96 mN/kW at 100 V, 2.5 A discharge.⁴ These designs have demonstrated an optimized in channel magnetic field will increase performance. Published knowledge acquired from these activities is incorporated into the design of the magnetic field in the modified T-220HT, herein referred to as the Embedded Electrode Hall Effect Thruster (EEHET).

The EEHET includes embedded graphite electrodes and an additional pair of electromagnets to generate a shielding field around the electrodes. The thruster is tested on xenon propellant on an inverted pendulum thrust stand and the results show increased performance in thrust, T/P ratio, I_{sp} , and anode efficiency. The mechanism for the increased performance is not yet understood. A study of the near field plume is necessary to gain an understanding of the physics. The goal of the work presented here is to determine the effect of the in-channel electrodes on the plume plasma. The electrodes generate an electric field near the channel surface that should repel ions that come in contact with the field. This should divert ions to a more axial path. This reduces ion-wall neutralization which increases ion density and decreases the plume divergence angle. The plume divergence angle is determined through ion current density measurements in the plume. A retarding potential analyzer (RPA) is used

¹ Graduate Student, Aerospace Engineering, 270 Ferst Dr NW, Student Member AIAA.

² Associate Professor, Aerospace Engineering, 270 Ferst Dr NW, Associate Fellow AIAA.

to measure ion energy distribution function through the plume to determine the effect of the electrodes on the acceleration mechanism.

II. Experimental Setup

A. Hall Thruster

All experiments are performed on a modified Pratt & Whitney T-220HT Hall thruster. Extensive testing has mapped the performance of the thruster over a power range of 2-22 kW at discharge voltages of 200-600 V.⁶ The T-220HT has a mean channel diameter of 188 mm, channel depth of 65 mm, and nominal power rating of 10 kW.

An Electric Propulsion Laboratory 375 series cathode is located at the 12 o'clock position of the thruster and declined approximately 40 degrees to the horizontal to be aligned with the local magnetic field. The cathode orifice is located approximately 1.5 cm downstream from the thruster exit plane. The cathode flow rate is set to 1 mg/s for all cases investigated. The discharge channel of the thruster is made of M26 grade boron nitride. A more detailed description of the T-220HT and its characteristics can be found in Ref. 6.

The T-220HT HET discharge supply is a 45-kW Magna-Power TSA800-54 power supply, and all other thruster components are powered with TDK-Lambda 1 or 3.3 kW Genesys power supplies. All electrical connections enter the chamber through separate feedthroughs. The thruster discharge supply is connected to a filter consisting of a 1.3 Ω resistance and 95- μ F capacitor. The filter acts as a low pass filter preventing oscillations in the current over 1.4 kHz from reaching the discharge supply. High-purity (99.999%) xenon propellant is supplied to the thruster via stainless steel lines. MKS 1179A mass flow controllers meter the propellant flow to the cathode and anode with an uncertainty of ± 0.03 and ± 0.2 mg/s, respectively. The flow controllers are calibrated by measuring gas pressure and temperature as a function of time in a known control volume.

B. Ion Focusing

Ion focusing is achieved with the application of positively-biased electrodes embedded in the inner and outer channel surfaces. The electrodes are biased above anode potential. The resultant electric fields repel off-axis ions and reduce wall collisions. However, the positive bias also causes the electrodes to collect a large amount of electron current. This may result in a performance loss as the overall discharge current would increase due to increased electron current on the electrodes. To reduce electron collection, cusp-shaped magnetic fields are placed over the electrodes. The cusp fields trap electrons being accelerated toward the electrodes and thus reduce collected current. The static magnetic fields in the thruster are analyzed in MagNet by Infolytica, and modified to create the cusp magnetic fields along specific sections of the channel wall. The target strength of the cusp field is determined by the Larmor radius of electrons, and in this case requires 95 G for an assumed 25 eV electron with a 1-mm radius.

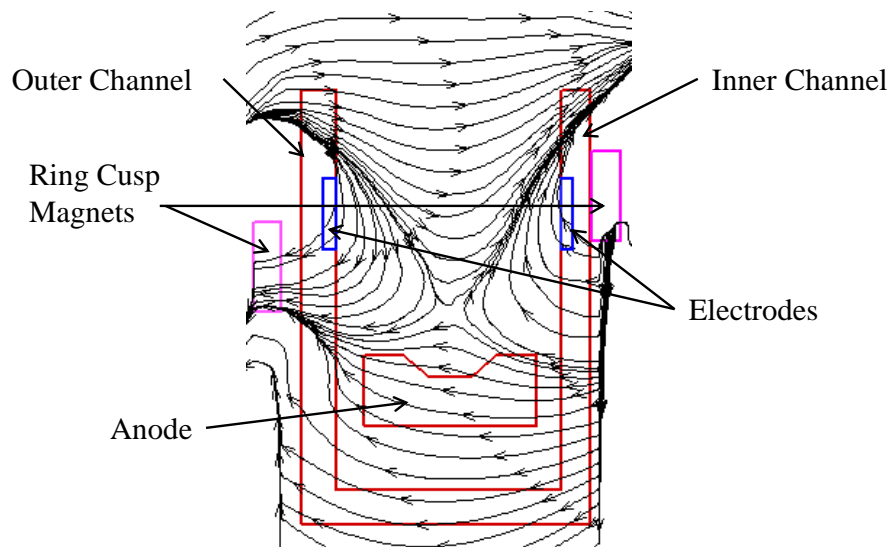


Figure 1. Simulated magnetic field for the redesigned thruster.

Figure 1 shows the resultant 2-D magnetic field, and the magnetic field is confirmed with physical Gauss probe measurements. **Figure 2** shows a schematic of the electrode electrical connections.

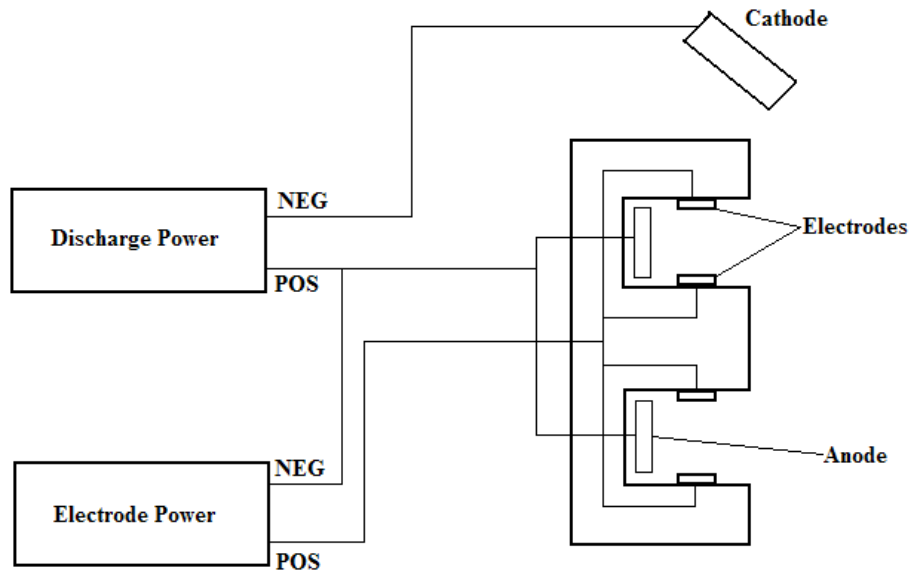


Figure 2. T-220HT electrical schematic.

C. Thrust Stand

Thrust is measured with a null-type inverted pendulum thrust stand based on the NASA GRC design by Haag.⁷ The null-type stand holds the thruster at a constant position with use of PID-controlled solenoid coils that move a center magnetic rod. Thrust is correlated to the amount of current on the null-coil required to hold the thrust stand at zero. Thrust stand calibration is performed by loading and off-loading a set of known weights. The resultant linear curve of null-coil current versus weight is used as the conversion for thrust measurements. A copper shroud surrounds the stand and coolant is passed through to maintain thermal equilibrium. Further details of the thrust stand and its operation can be found in Ref. 7.

D. Faraday Probe

A Faraday probe is a simple plasma diagnostic used to measure ion current density in the HET plume. Its use has been well documented.^{2, 8-11} Figure 3 shows a picture and electrical schematic of the Faraday probe used in this work. The probe consists of a tungsten-coated, stainless-steel collection electrode with a stainless-steel guard ring surrounding it, with a 0.12 cm gap between. The collector and guard ring are both biased to 20 V below ground to repel electrons. Biasing the collector and guard ring to the same potential reduces edge effects by creating a uniform sheath potential around the collector. The collector disk is 2.31 cm in diameter. A Lambda GENH 60-12.5 power supply biases the collector and shield to 20 V below ground. A 1.417 k Ω , 0.5 W resistor is placed in series with the collector line and voltage across the resistor is read by an Agilent 34980A data acquisition unit. The probe is mounted above the thruster, and centered over the exit plane. The collector surface is placed 1 meter downstream of the thruster exit plane. Sweeps are taken from -100 to +100 degrees from thruster centerline in one degree increments. Measurements were taken at 80 Hz sample rate for one second at each position and averaged to produce the recorded current density at that location.

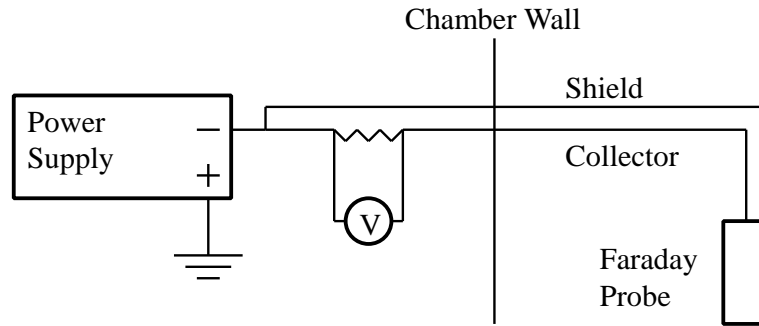


Figure 3. Faraday probe of JPL design.²

E. Retarding Potential Analyzer

A retarding potential analyzer (RPA) measures ion energy per charge with a series of biased grids to selectively filter ions.^{12, 13} The RPA cannot discriminate between singly- and doubly-charged ions. An RPA acts as a high-pass filter that only allows ions with energy higher than the ion repulsion grid to pass through to the collector. By increasing the voltage on the ion retarding grid, ions with equal or less energy are repelled and the collect current drops. The derivative of the resulting current-voltage data is proportional to the ion energy distribution function $f(V)$ by Eq. (1).¹²

$$\frac{dI}{dV} = -\frac{Z_i^2 e^2 n_i A_c}{m_i} f(V) \quad (1)$$

The RPA used in this work, along with an electrical schematic, is shown in Figure 4. The RPA uses four grids and a collector. In order, they are the floating, electron repulsion, ion repulsion, and electron suppression grids. The floating grid charges to the plasma potential to reduce perturbations caused by the probe presence. The electron repulsion grid is negatively biased with respect to ground to repel plasma electrons, and the ion repulsion grid is positively biased with respect to ground to retard ions. The electron suppression grid is biased negative with respect to ground to repel any secondary electrons emitted from the collector due to ion collisions. The electron repulsion and suppression grids are both biased to -30 V by a pair of GENH 60-12.5 power supplies. The ion repulsion grid is powered by a Keithley 2410 Sourcemeater. The collector current is measured with a Keithley 6487 Picoammeter. Both the sourcemeater and picoammeter are controlled via LabVIEW.

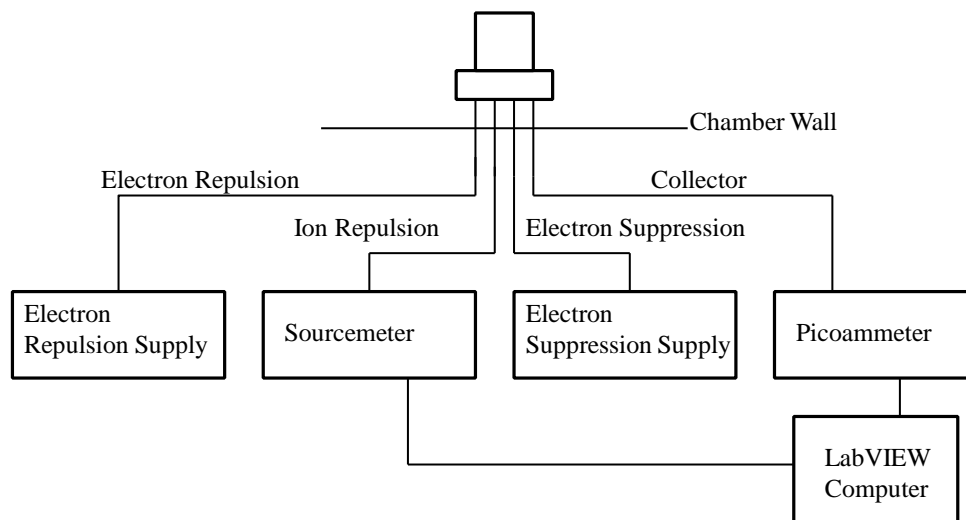
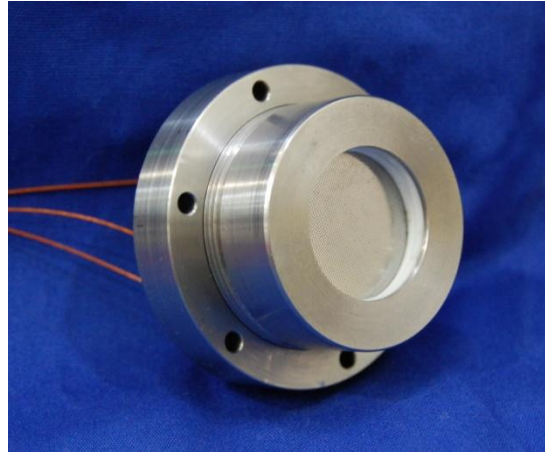


Figure 4. Four-grid RPA.¹

F. Floating Emissive Probe

The ion energy distribution obtained from RPA is measured with respect to ground, but the ions are referenced with respect to the plasma potential. To correct the RPA measurements, the plasma potential is needed. To measure the plasma potential, a floating emissive probe is used. Emissive probes are a widely used plasma diagnostic to measure the plasma potential. The probe consists of a thermally emissive filament loop housed in a ceramic insulator. A Xantrex XPD 60-9 power supply applies current and heats the filament to the point of thermionic emission of electrons. When exposed to the plasma, any probe naturally floats from ground to the floating potential. At the floating potential a sheath forms around the probe and there is no net current to the probe. This is due to the negative plasma electron current balanced by the positive plasma ion current and secondary electron emission. However, because the emissive probe emits its own electrons, the probe becomes more positive, which in turn draws in more plasma electrons. This process continues until the probe potential reaches the plasma potential.

The measured plasma potential is subtracted from the RPA measurement, shifting the RPA results to lower potential. This corrects for artificially high ion energies due to the aforementioned ground/plasma potential referencing. The emissive probe used in this work consists of a 1.5 mm diameter thoriated-tungsten filament housed in a double-bored alumina tube based on ones used by Haas.¹⁴ The filament loop has a radius of 1.5 mm. Figure 5 shows a schematic of the probe. The voltage reading between probe and ground is taken with the Agilent 34980A data acquisition unit at the same time as RPA measurements are taken, averaging 400 points.

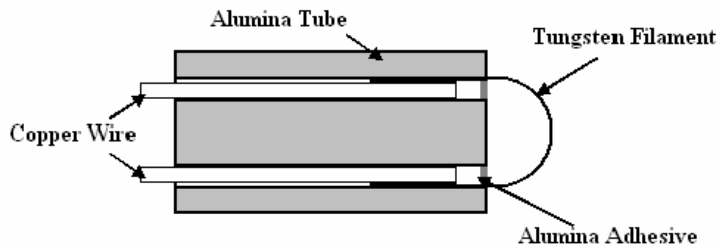


Figure 5. Emissive probe.

G. Vacuum Facility

All experiments are performed in the Vacuum Test Facility 2 (VTF-2) shown in Figure 6. VTF-2 is 9.2 meters long and 4.9 meters in diameter. It is pumped to rough vacuum with one 3800 CFM blower and one 495 CFM rotary-vane pump. Ten liquid nitrogen cooled CVI TMI re-entrant cryopumps with a combined pumping speed of 350,000 l/s on xenon bring the chamber to a base pressure of 5×10^{-9} Torr. A Stirling Cryogenics SPC-8 RL Special Closed-Looped Nitrogen Liquefaction System supplies liquid nitrogen to the cryopump shrouds. MKS 1179A mass flow controllers meter the propellant and a constant volume calibration system is used to calibration the mass flow rate. Two ionization gauges, Varian 571 and UHV-24, are mounted on either side of the chamber.

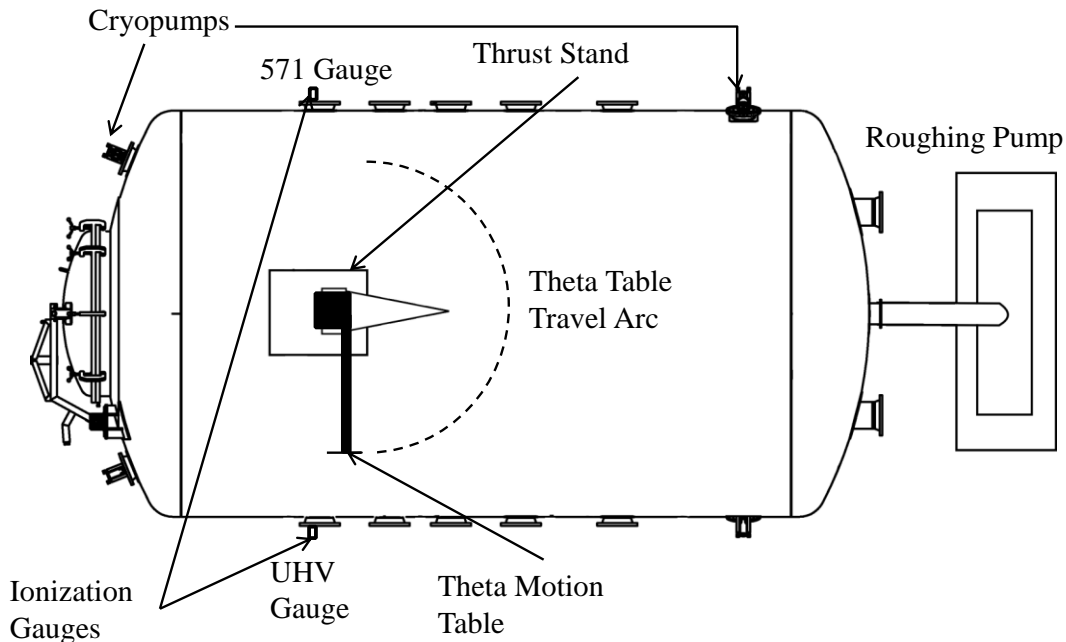


Figure 6. Schematic of VTF2 (not to scale).

III. Results

The thruster is operated over 125-300 V discharge voltage at 9 ± 0.1 A. The electrodes are tested at three setting, electrically floating, biased to 10 V and 30 V above anode potential. These three settings are noted as Floating, $10 V_e$, and $30 V_e$ respectively from here on. Magnet currents remain constant through all tests to provide the field topography shown in Figure 1. The thruster is run through a one hour conditioning cycle before data are taken. Figure 7 and Figure 8 shows the performance (thrust, T/P ratio, I_{sp} and anode efficiency) of the EEHET running on xenon at 9 A. Additionally, data for a no electrode configuration are shown as well. In this case, labeled as BN in

the data, the graphite electrodes are replaced with BN rings to approximate the original discharge channel. The power used in the T/P ratio and efficiency calculations is the total discharge power, which includes both anode and electrode powers. The floating and BN data fall within close proximity with each other, indicating the addition of the embedded electrodes has a minor effect on the thruster. The thruster performance increased along all four metrics with biased electrodes. T/P and efficiency are higher at 10 V_e than at 30 V_e . The 30 V_e case has larger increases in thrust than 10 V_e , however there is a large increase in electrode power at 30 V_e , which reduces the T/P ratio and efficiency. The maximum total T/P ratio increase occurs at 175 V discharge, resulting in a gain of 4.2 mN/kW, 135 s of I_{sp} , and 6% efficiency. Chamber pressure is between $9 \times 10^{-6} - 1.5 \times 10^{-5}$ Torr-Xe for all tests.

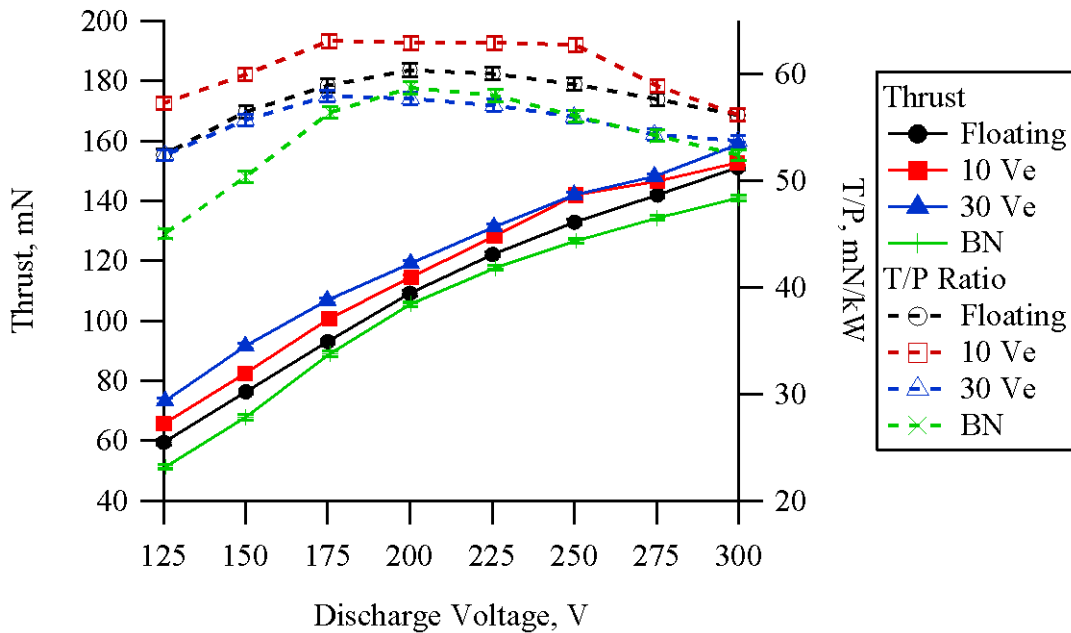


Figure 7. Thrust and T/P ratio at 9 A on xenon at Floating, 10 V_e , 30 V_e , and BN rings.

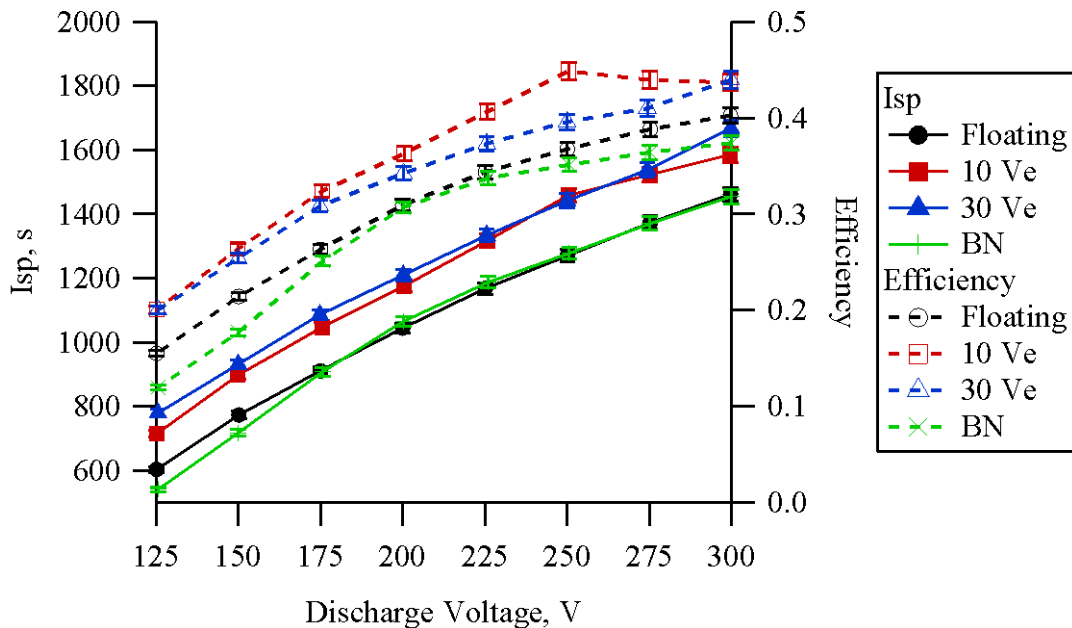


Figure 8. Specific impulse and anode efficiency at 9 A on xenon at Floating, 10 V_e , 30 V_e , electrode bias and BN rings.

Plume measurements are taken at the same operation conditions as Figure 7 and 8, namely 125-300 V and 9 A discharge with floating, 10 V_e and 30 V_e . All three probes are placed 1 meter downstream of the thruster exit plane on a radial motion arm centered above the exit plane. There is a 5-degree separation between each probe. The probes are aligned to thruster center with a laser tool. Faraday traces of the ion current density are done from +100 to -100 degrees. Figure 9 shows the measured ion current density for the floating case at 125-300 V and 9 A discharge. The mass flow rate varied from 10.02 to 10.36 mg/s to maintain current as shown in Table 1.

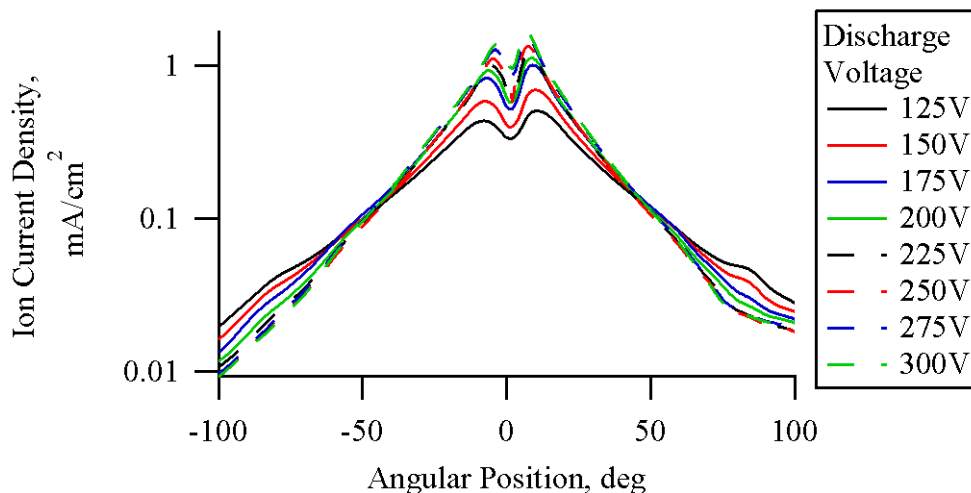


Figure 9. Current density map for 125-300 V discharge with floating electrodes at 9 A .

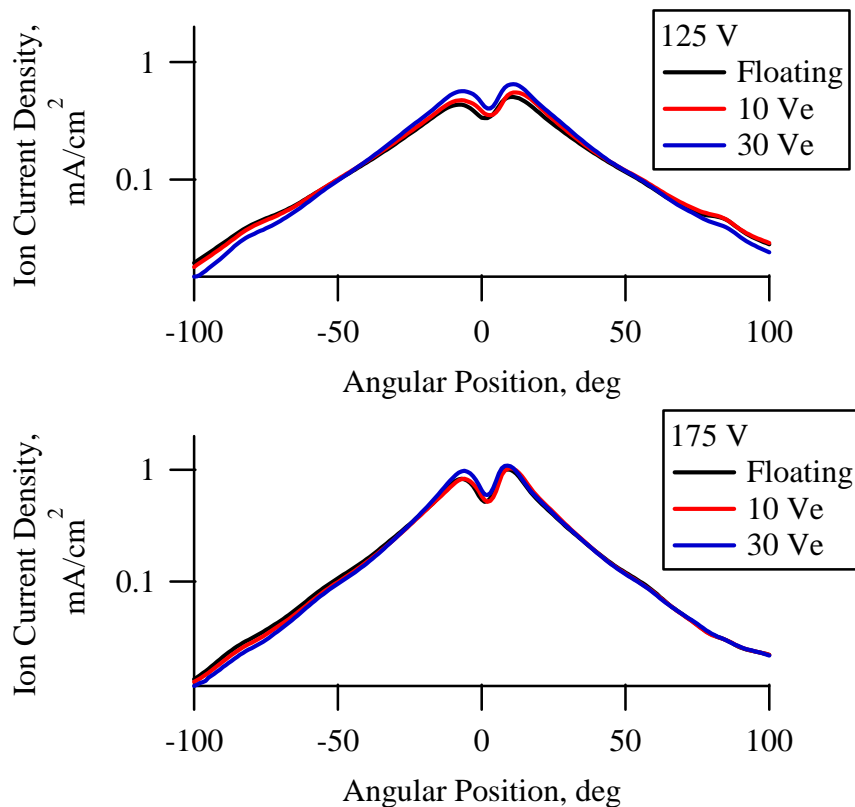
Table 1. Operating conditions for data presented.

Discharge Voltage	Floating		10 V_e		30 V_e	
	Mass Flow, mg/s	Id, A	Mass Flow, mg/s	Id, A	Mass Flow, mg/s	Id, A
300	10.02	9.12	9.91	9	9.80	8.98
275	10.02	9.03	10.02	8.97	9.80	8.97
250	10.02	8.97	10.02	9.1	9.91	9.03
225	10.14	8.92	10.14	9	9.91	8.98
200	10.36	8.93	10.36	9.02	10.02	8.9
175	10.36	8.98	10.25	9.02	10.14	8.98
150	10.14	8.9	9.91	9.08	9.91	8.93
125	10.25	8.93	9.80	9	9.80	8.9

The T-220HT thruster exhibits a double peak structure which signifies the focal length is longer than 1 meter. The peaks rest between 6-9 degrees on either side of centerline. The exact peak location varies depending on operating conditions. The asymmetry of the peaks can be attributed to blockage of the propellant distributor holes at certain locations and imperfect alignment. The current densities decrease with discharge voltage and thus acceleration and ionization capability decreases, resulting in fewer ions. All data are taken at discharge currents between 8.9 – 9.12 A as shown in Table 1, thus lower voltages sees an increase in electron current. Figure 10 shows the change in the current density with biased electrodes for 125, 175, 225 and 300 V. The 10 V_e case shows a minor change from the floating case, but 30 V_e creates a noticeable change in the current density. The current density trend upwards as discharge voltage is increased, which is expected. The current density increases at small angles resulting in larger peaks and decreases at large angles. The increase at small angles without a net upward shift of the

plot indicates an increase in the ion density specifically in that region as opposed to everywhere. This is further supported by the decrease at large angles. Figure 11 shows a magnified view of the same data at large angles.

At any given voltage, the discharge current is kept approximately constant and the magnet settings are the same. The only difference is the electrode power. As electrode bias increases, so does the current seen by the electrodes. The average electrode current at 10 V_e and 30 V_e are 1.5 and 9.2 A respectively. The increase in the ion flux around centerline and decreases in the wings can be attributed to a narrowing of the ion beam and decreased plume divergence angle. Figure 12 plots the plume divergence angle for all three cases (Floating, 10 and 30 V_e). The divergence angle was calculated by taking a linear fit of the 10-30 degree data on a semi-log plot and extrapolating it to 90 degrees.¹⁵ This removes charge exchange ion contribution to the current density. Trapezoidal integration is used to find the area under the curve. Numerical interpolation is then used to determine the 90% beam current angle on the right and left sides. The right and left angles are then averaged to produce the final divergence angle. The angles are larger than typical for a modern HET. This is largely due to the magnetic field placement and the plasma lens existing just beyond the exit plane of the thruster. The accelerated ion can have a wider angle due to lack of a wall. There are minor changes in plume divergence angle from floating to 10 V_e , but at 30 V_e the plume angle decreases by up to 6 degrees. Along with the increase in thrust observed, this suggests either increased axial ion velocities or increased ion count.



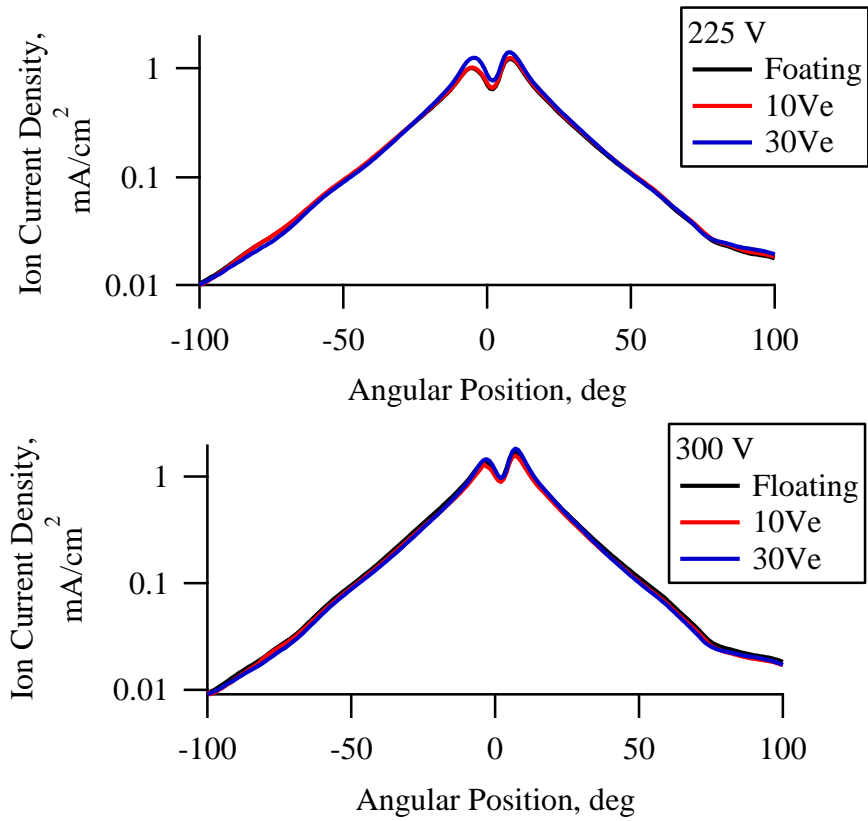


Figure 10. Ion current density profile for operating conditions of (125 V, 8.93 A), (175 V, 8.98 A), (225 V, 8.98 A), and (300 V, 9 A) for electrode bias configurations floating, 10 V, and 30 V.

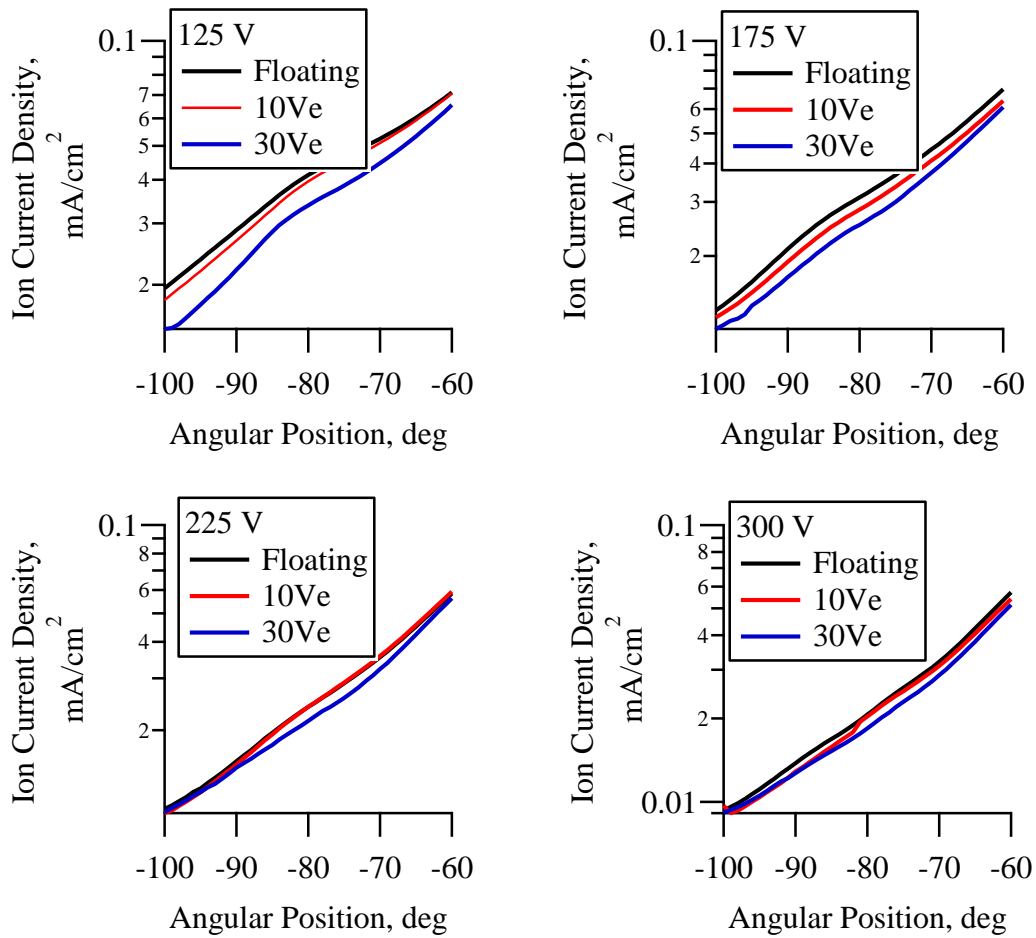


Figure 11. Close up ion current density profiles from Figure 10, from 60 to 100 degrees of chamber centerline.

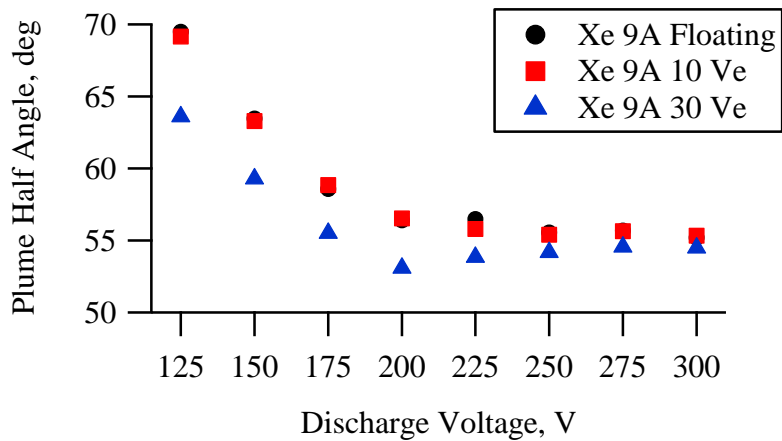


Figure 12. Plume divergence half angle for 90% of total beam.

Ion energy and plasma potential measurements are taken with the RPA and emissive probe at 10 locations around the plume. From 0 to 30 degrees measurements are taken in 5-degree increments and from 40 to 60 degrees in 10 degree increments. One RPA sweep at each location was taken, however at each ion repulsion grid potential setting three measurements were taken and averaged. A 4th order Savitzky-Golay smoothing filter was applied to the raw data prior to taking the derivative. Figure 13 shows the ion energy distribution function on thruster on thruster centerline. The profile shows that the ion energy distribution function broadens as the discharge voltage increases. This is expected as high voltages result in increased ionization across the acceleration region and thus a larger spread in possible ion energies.

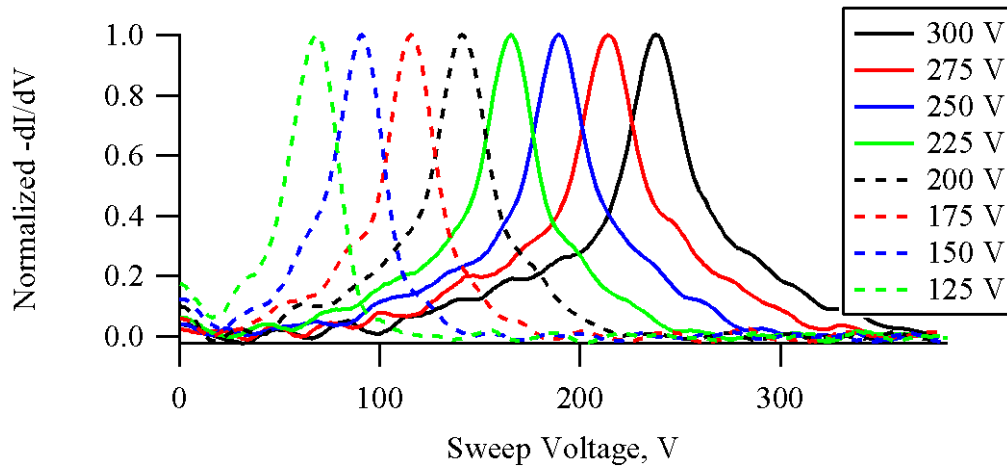


Figure 13. Ion energy distribution function on thruster centerline for floating electrodes at 9 ± 0.1 A.

Figure 14 shows the computed ion energy distribution function when the thruster is operating at 175 V and 9 A for all three electrode cases at four angular locations. The biased electrodes generate a shift in ion energy distribution function to higher voltages. Similar trends are observed for other discharge voltages. At $10 V_e$, there is a slight rightward shift of the ion energy distribution, on the order of a few volts. At $30 V_e$, the shift is an average of 20 V. Figure 15 plots the most probable ion energy for the 175 V operating condition at all measured angles. There is a definite change in behavior from $10 V_e$ to $30 V_e$ which will be discussed in the next section. The ion energy distribution also widens with increased electrode bias. The widening decreases at larger angles. This means the electrodes increase the spread of ion energies at small angles to centerline. This can be caused either by increased ionization potential which would generate a large spread, or focusing of lower energy ions towards small angles. The latter seems more likely as the widening is significant only at small angles. If base ionization potential is increased, the ion energy distribution function would be broader everywhere.

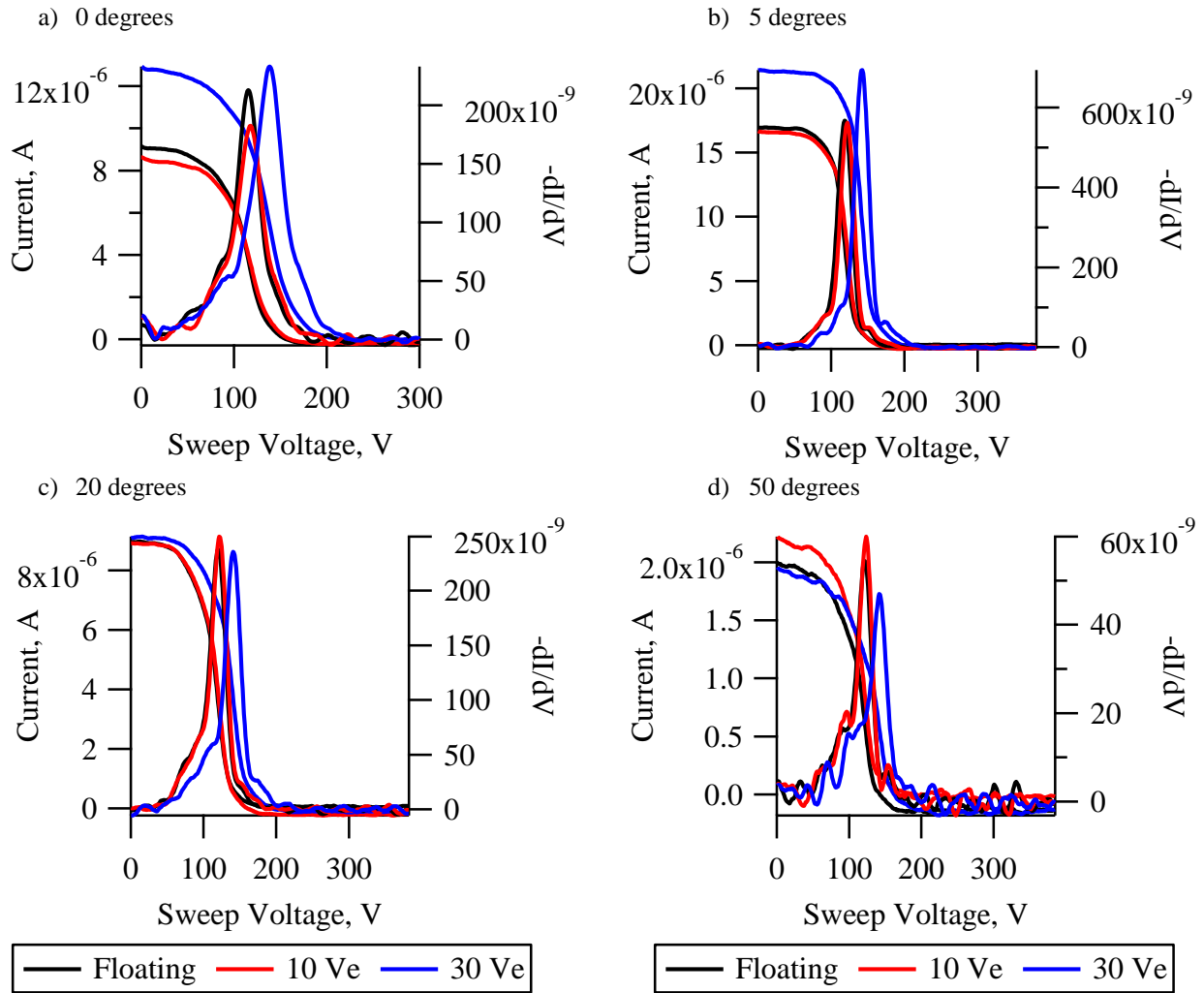


Figure 14. Ion energy distribution function with electrodes at 175 V discharge voltage at various angular

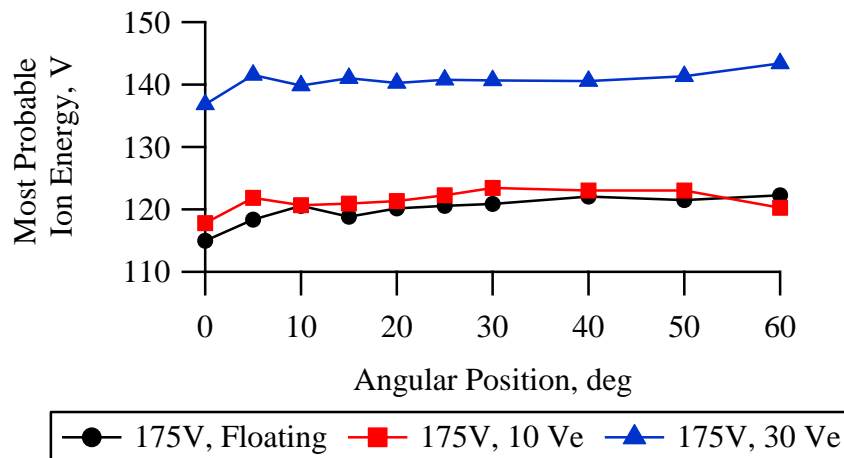


Figure 15. Most probable ion energy for the ion energy distribution function at each measured angle on xenon at 175 V and Floating (8.98 A discharge), 10 Ve (9.02 A), and 30 Ve (8.98 A).

IV. Discussion

The goal of this work is to reduce ion-wall neutralization, plume divergence, and increase the ion number density. Evidence that this has occurred would present as an increased ion current density for the same propellant and a more collimated ion beam. Evidence of a tighter or more collimated ion beam is a decrease in the plume divergence angle, and increase in ion density at small angles from thruster centerline, and a decrease in ion current density at large angle. As Figure 12 shows, there is indeed a decrease in the plume divergence angle when the electrodes are biased above anode potential. This divergence angle decrease is not unexpected as previous work done with secondary electrodes in the discharge channel also shows a decreased plume divergence angle.^{16,17} At 10 V_e the effect is very minor, typically less than one degree half angle. At 30 V_e the plume divergence half angle decreases by up to six degrees. The current density profiles increase around the centerline of the thruster and decrease at large angles as electrode bias is increased. The change is small at 10 V_e, and larger at 30 V_e. The integration of the beam current also shows a similar trend. Figure 16 shows the integrated beam current divided by the discharge current, I_i/I_d . There is an overall increase in the total ion current as electrode potential increases. Figure 17 shows the mass flow rates for the current fractions in Figure 16. As the thruster was operated at constant current, the mass flow rate changed to match. The cathode flow rate was kept constant, and as Figure 17 shows, the anode flow rate either stayed constant, or decreased as electrode bias increased. Coupled with increase current fraction, this means the increased ion beam fraction is caused by an increased number of ions as opposed to more propellant neutrals. This equates to increased mass utilization.

Increased beam current fraction is the result of increase ion density. Two possible explanations for the increase density are increased ionization or reduction in ion losses. The electrodes are located upstream of the ionization/acceleration regions near the plasma lens, so they are unlikely to have a significant impact on ionization. The effect is greater at lower discharge voltages because a 30 V potential has a greater effect on a 125 V ion compared to a 300 V one by simple vector addition. This points to electrodes repelling ions from the walls, and a reduction in ion-wall neutralizations.

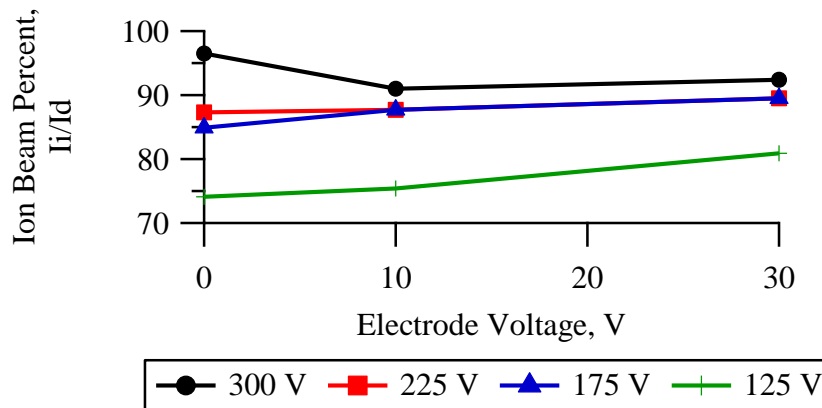


Figure 16. Ion beam current percentage, I_i/I_d .

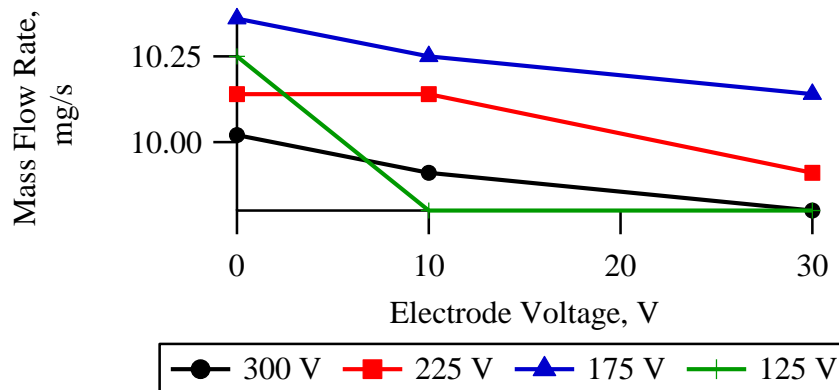


Figure 17. Mass flow rate for 125, 175, 225, and 300 V at various electrode conditions.

It is important to note that the ion energy distribution functions increases as the electrode bias increases. Figure 18 shows the most probable ion energy for the various test conditions in Figure 16 Figure 17. At 10 V_e the increase in ion energy is small, less than 6.3 V at the maximum. At 30 V_e the increase ranges from 19 to 25 V. Though the increase in ion energy is small at 10 V_e , combined with the decrease in divergence angle results in a significant increase in thrust and T/P ratio over the floating case (up to 7.6 mN and 4.2 mN/kW). At 30 V_e the thrust increases even more (up to 13.7 mN), however the electrodes also see a marked increase in collected current, which leads to a reduction in the T/P (loss of 1-3 mN/kW). Figure 19 shows the electrode collected current. At 10 V_e , the electrode current is higher at both ends of the discharge voltage test range, but at 30 V_e the current is relatively constant across the test range. This suggests that at the lower electrode bias the electrode effect on the plasma depends on other factors while at higher bias the plasma reaches some steady state. This means there are possibly two different modes of operation or behaviors that depend on electrode bias. At 10 V_e the electrodes may be primarily focusing ions, pushing energetic ions towards centerline. However, the larger increase at 30 V_e suggests an acceleration mechanism, in addition to or instead of ion focusing, is in effect. The electrodes may become the primary anode at this point. However the current on the main anode did not change significantly. Current was not shifted from anode to electrodes, which contradicts the idea of the electrodes as primary anode.

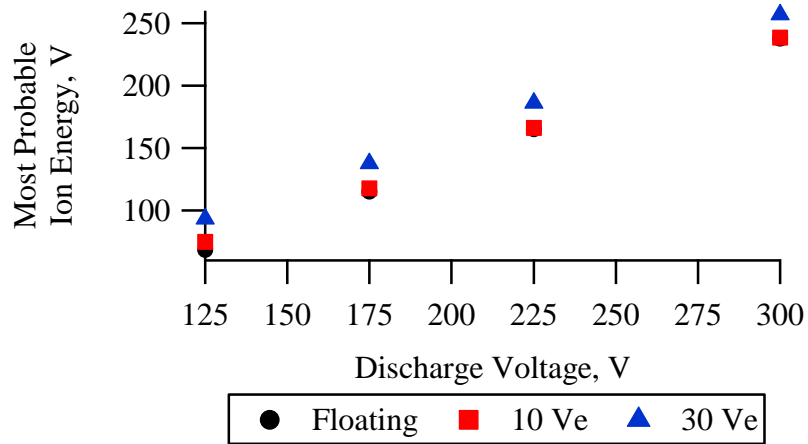


Figure 18. Most probable ion energy for 125, 175, 225, and 300 V at 9 A and various electrode conditions.

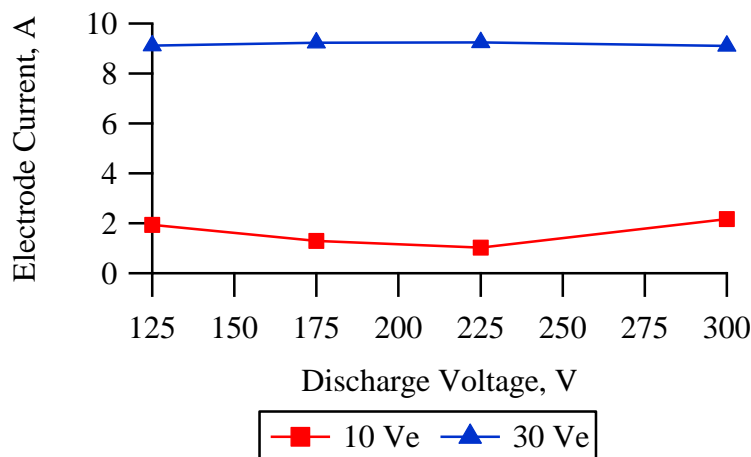


Figure 19. Electrode current for 125, 175, 225, and 300 V at 9A and 10 and 30 V electrode bias.

One possible explanation of the difference from floating to 10 and then to 30 V_e is expansion of the plasma sheath. At 10 V_e the plasma sheath surrounding the electrode shields out the electric field from the majority of the

plasma. The electrode thus only affects a small fraction of the plasma. Once the electrodes increase to 30 V_e though, their electric field reaches out further and is able to affect a larger portion of the bulk plasma. This would require an increase in the sheath thickness. Anders showed with a DC-biased flat substrate that the sheath thickness does increase with surface bias.¹⁸ In that work however the substrate was biased to many kilovolts of potential and the sheath increase was on a few millimeters, but the relation is likely still valid at lower voltages.

Another contribution to sheath thickness could be the near-wall magnetic fields. The static magnetic field in Figure 1 shows cusp fields surrounding the two electrodes. The intent of these fields is to reduce electron collection. A secondary effect of oblique or parallel fields near a surface is the extension and enlargement of the near-wall sheath. Research has shown that magnetic fields next to wall surfaces can increase the thickness of the plasma sheath.¹⁹⁻²² In the probe data presented, the magnets were kept constant and thus the magnetic field effects on the sheath can be assumed the same between 10 V_e and 30 V_e. Preliminary test of the thruster with different ring cusp magnet settings does show a change in electrode current with magnet settings. Figure 20 shows the electrode current measured as the shielding ring-cusp magnets were increased. The electrode current decreases at first in response to increased field strength around the electrodes which decrease electron transport, however it rises again when the magnets are brought up to 15A. This behavior indicates a secondary phenomenon occurring at high enough magnetic field strength besides trapping of electrons on field lines. The two effects of a biased surface and near-wall cusp magnetic field could in part explain the changes seen in ion energy. In-channel measurements of the near-wall plasma are necessary to further pursue this line of analysis.

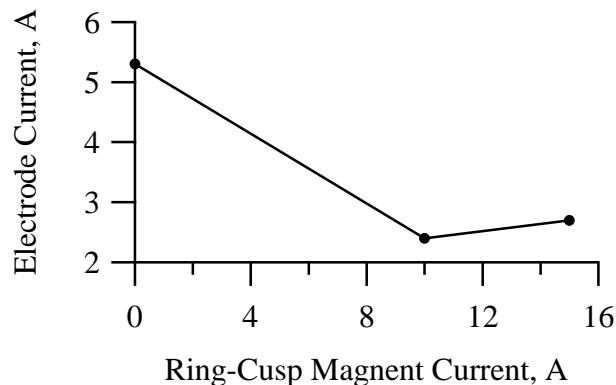


Figure 20. Electrode current at various ring-cusp shielding magnet currents at 175 V, 9 A discharge and 20 V_e.

V. Conclusion

This work shows that the addition of focusing electrodes in the discharge channel has positive effects on Hall thruster performance. The thruster is tested on xenon at 9 A at several combinations of discharge voltage and electrode bias voltage. The electrodes cause a definite increase in thruster performance across all four metrics of thrust, total *T/P* ratio, anode efficiency, and specific impulse at 10 V electrode bias. Plume measurements show an increased current density at small angles to centerline and decrease at large angles. Along with increase ion beam current fraction, this points to an increased ion number density, specifically near the centerline of the thruster. The goal to decrease ion-wall neutralization and plume divergence losses by biasing the electrodes above anode potential to force the off-axis ions away from the discharge chamber walls seems to have been accomplished.

The RPA data shows increased most probable ion energy. The increase is small at 10 V_e and much larger at 30 V_e. As the discharge conditions were not changed, this means the electrodes provided an additional acceleration to the ions in addition to any ion focusing. The increased ion current fraction with constant or decreasing mass flow means an increased mass utilization with electrode bias. The difference in level of ion energy change between the two electrode conditions leads to the conclusion the thruster is operating in two different modes, dependent on electrode bias. The biased electrode may extend the near-wall plasma sheath thickness as seen by other researchers. An increased plasma sheath due to near-wall cusp magnetic fields may also have a part in the observed differences, but the plume plasma response to a changing magnetic field data was not taken here. Further study of the in-channel discharge plasma is required to better understand the observed behaviors.

Acknowledgments

The research contained herein is sponsored by American Pacific In-Space Propulsion. We would like to thank Pratt & Whitney for supplying HPEPL with the T-220HT, Gregory McCormick for work in simulation and modifications, Hoang Dao for programming assistance, and departmental technical staff and other graduate students at HPEPL for assistance with this work. Kunning Xu is supported by the National Defense and Science Engineering Graduate Fellowship and the Georgia Institute Fellowship. The authors are greatly appreciative of this support.

References

- ¹Brown, D. L. "Investigation of Low Discharge Voltage Hall Thruster Characteristics and Evaluation of Loss Mechanism," *Aerospace Engineering* Vol. Ph.D. Dissertation, University of Michigan, Ann Arbor, MI, 2009.
- ²Walker, M. L. R., Hofer, R. R., and Gallimore, A. D. "The Effects of Nude Faraday Probe Design and Vacuum Facility Backpressure on the Measured Ion Current Density Profile of Hall Thruster Plumes," *38th AIAA Joint Propulsion Conference*. Vol. AIAA 2002-4253, Indianapolis, IN, 2002.
- ³Hofer, R. R. "Development and Characterization of High-Efficiency, High-Specific Impulse Xenon Hall Thrusters," *Aerospace Engineering*. Vol. Ph.D. Dissertation, University of Michigan, Ann Arbor, MI, 2004.
- ⁴Pote, B., and Tedrake, R. "Performance of a High Specific Impulse Hall Thruster," *27th International Electric Propulsion Conference*. Vol. IEPC-01-35, Pasadena, CA, 2001.
- ⁵de Grys, K., Rayburn, C., Wilson, F., Fisher, J., Werthman, L., and Khayms, V. "Multi-Mode 4.5 kW BPT-4000 Hall Thruster Qualification Status," *39th AIAA Joint Propulsion Conference*. Vol. AIAA 2003-4554, Huntsville, AL, 2003.
- ⁶McVey, J. B., Britt, E. J., Engelman, S. F., Gulczynski, F. S., Beiting, E. J., and Pollard, J. E. "Characteristics of the T-220HT Hall-Effect Thruster," *39th Joint Propulsion Conference*. Vol. AIAA 2003-5158, Huntsville, AL, 2003.
- ⁷Xu, K. G., and Walker, M. L. R. "High-Power, Null-Type, Inverted Pendulum Thrust Stand," *Review of Scientific Instruments* Vol. 80, 2009.
doi: 10.1063/1.3125626
- ⁸Manzella, D. H., and Sankovic, J. M. "Hall Thrusters Ion Beam Characterization," *31th AIAA Joint Propulsion Conference*. Vol. AIAA 95-2927, San Diego, CA, 1995.
- ⁹Hofer, R. R., Walker, M. L. R., and Gallimore, A. D. "A Comparison of Nude and Collimated Faraday Probes for Use with Hall Thrusters," *27th International Electric Propulsion Conference*. Vol. IEPC-01-020, Pasadena, CA, 2001.
- ¹⁰Mason, L. S., and Jankovsky, R. S. "1000 Hour of Testing on a 10 Kilowatt Hall Effect Thruster," *37th AIAA Joint Propulsion Conference*. Vol. AIAA 2001-3773, Salt Lake City, UT, 2001.
- ¹¹Brown, D. L., and Gallimore, A. D. "Evaluation of Facility Effects on Ion Migration in a Hall Thruster Plume," *Journal of Propulsion and Power* Vol. 27, No. 3, 2011, pp. 573-585.
doi: 10.2514/1.B34068
- ¹²King, L. B. "Transport-Property and Mass Spectral Measurements in the Plasma Exhaust Plume of a Hall-Effect Space Propulsion System," *Aerospace Engineering*. Vol. Ph.D. Dissertation, University of Michigan, Ann Arbor, MI, 1998.
- ¹³Hutchinson, I. H. *Principles of Plasma Diagnostics*. Cambridge: Cambridge University Press, 1987.
- ¹⁴Haas, J. M. "Low-Perturbation Interrogation of the Internal and Near-Field Plasma Structure of a Hall Thruster Using a High-Speed Probe Positioning System," *Aerospace Engineering*. Vol. Ph.D. Dissertation, University of Michigan, Ann Arbor, MI, 2001.
- ¹⁵Hofer, R. R., Jankovsky, R. S., and Gallimore, A. D. "High-Specific Impulse Hall Thrusters, Part 1: Influence of Current Density and Magnetic Field," *Journal of Propulsion and Power* Vol. 22, No. 4, 2006, pp. 721-731.
- ¹⁶Raitses, Y., Dorf, L. A., Litvak, A. A., and Fisch, N. J. "Plume Reduction in Segmented Electrode Hall Thruster," *Journal of Applied Physics* Vol. 88, No. 3, 2000, pp. 1263-1270.
- ¹⁷Kieckhafer, A. W. "The Effect of Segmented Anodes on the Performance and Plume of a Hall Thruster," *Mechanical Engineering*. Vol. Ph.D. Dissertation, Michigan Technological University, Houghton, MI, 2007.
- ¹⁸Anders, A. "Width, Structure and Stability of Sheaths in Metal Plasma Immersion Ion Implantation and Deposition: Measurements and Analytical Considerations," *Surface and Coating Technology* Vol. 136, 2001, pp. 85-92.
- ¹⁹Cohen, R. H., and Ryutov, D. D. "Plasma Sheath in a Tilted Magnetic Field: Closing of the Diamagnetic Currents; effect on Plasma Convection," *Physics of Plasmas* Vol. 2, No. 6, 1995, pp. 2011-2019.
- ²⁰DeWald, A. B., Bailey, A. W., and Brooks, J. N. "Trajectories of Charged Particles Traversing a Plasma Sheath in an Oblique Magnetic Field," *Physics of Fluids* Vol. 30, No. 1, 1986, pp. 267-269.
- ²¹Anders, A., Anders, S., and Brown, I. G. "Effect of Duct Bias on Transport of Vacuum Arc Plasmas Through Curved Magnetic Filters," *Journal of Applied Physics* Vol. 75, No. 10, 1994, pp. 4900-4905.
- ²²Keidar, M., and Beilis, I. I. "Plasma-Wall Sheath in a Positive Biased Duct of the Vacuum Arc Magnetic Macroparticle Filter," *Applied Physics Letters* Vol. 73, No. 3, 1998, pp. 306-308.